

3D Printing multifunctionality: structures with electronics

David Espalin · Danny W. Muse · Eric MacDonald ·
Ryan B. Wicker

Received: 4 July 2013 / Accepted: 10 February 2014 / Published online: 4 March 2014
© Springer-Verlag London 2014

Abstract While NASA explores the power of 3D printing in the development of the next generation space exploration vehicle, a CubeSat Trailblazer was launched in November 2013 that integrated 3D-printed structures with embedded electronics. Space provides a harsh environment necessary to demonstrate the durability of 3D-printed devices with radiation, extreme thermal cycling, and low pressure—all assaulting the structure at the atomic to macroscales. Consequently, devices that are operational in orbit can be relied upon in many terrestrial environments—including many defense and biomedical applications. The 3D-printed CubeSat module (a subsystem occupying approximately 10 % of the total volume offered by the 10×10×10-cm CubeSat enclosure) has a substrate that fits specifically into the available volume—exploiting 3D printing to provide volumetric efficiency. Based on the best fabrication technology at the time for 3D-printed electronics, stereolithography (SL), a vat photopolymerization technology, was used to fabricate the dielectric structure, while conductive inks were dispensed in channels to provide the electrical interconnect between components. In spite of the structure passing qualification—including temperature cycling, shock and vibration, and outgas

testing—the photocurable materials used in SL do not provide the level of durability required for long-term functionality. Moreover, the conductive inks with low-temperature curing capabilities as required by the SL substrate material are widely known to provide suboptimal performance in terms of conductivity. To address these challenges in future 3D-printed electronics, a next generation machine is under development and being referred to as the multi^{3D} system, which denotes the use of multiple technologies to produce 3D, multi-material, multifunctional devices. Based on an extrusion process necessary to replace photocurable polymers with thermoplastics, a material extrusion system based on fused deposition modeling (FDM) technology has been developed that integrates other technologies to compensate for FDM's deficiencies in surface finish, minimum dimensional feature size, and porosity. Additionally, to minimize the use of conductive inks, a novel thermal embedding technology submerges copper wires into the thermoplastic dielectric structures during FDM process interruptions—providing high performance, robust interconnect, and ground planes—and serendipitously improving the mechanical properties of the structure. This paper compares and contrasts stereolithography used for 3D-printed electronics with the FDM-based system through experimental results and demonstrates an automated FDM-based process for producing features not achievable with FDM alone. In addition to the possibility of using direct write for electronic circuitry, the novel fabrication uses thermoplastics and copper wires that offer a substantial improvement in terms of performance and durability of 3D-printed electronics.

D. W. Muse
Printed Device Concepts, Inc, El Paso, TX, USA

E. MacDonald
Department of Electrical Engineering, The University of Texas at El Paso, El Paso, TX, USA

D. Espalin · R. B. Wicker
Department of Mechanical Engineering, The University of Texas at El Paso, El Paso, TX, USA

D. Espalin (✉) · E. MacDonald · R. B. Wicker
W.M. Keck Center for 3D Innovation, The University of Texas at El Paso, El Paso, TX, USA
e-mail: despalin@utep.edu

Keywords Additive manufacturing · 3D Structural electronics · Satellites · 3D Printing · Embedded components · Embedded wires · Conductive inks · Ultrasonic embedding · Laser microwelding

1 Introduction

Additive manufacturing (AM)—also known more popularly as 3D printing—brings to bear a freedom to design and fabricate 3D complex geometric structures that is unprecedented. Designs are captured in CAD and can be easily modified to enable reuse and unit-level customization. Currently, the majority of these AM technologies are relegated to a minimal number of materials in a given fabrication; however, research has begun to focus on more sophisticated systems with process interruption capabilities including (1) inserting components (electronics, magnetics, sensors, batteries, etc.) into specific cavities within fabricated structures [1–3], (2) dispensing widely disparate materials for specific functionalities (thermal and electrical conductivity, radiation shielding, optics, flame retardance, etc.) [1, 4–6], and (3) embedding solid conductors within polymer substrates through the use of ultrasonic or thermal energy in order to provide high-performance electrical interconnect [7, 8]. Integrated together these technologies are able to 3D print multifunctionality to produce complex functional electronic and electromechanical systems in an automated manner.

Inevitably, these new technologies will develop with improved dimensional accuracies. With improved process control, the integration of additional manufacturing technologies, and an increasingly wide range of materials options, these systems may eventually be able to 3D print a custom cell phone locally using a design purchased and downloaded from the internet. This profound shift in manufacturing—from remote factories to local 3D printing—will not only reduce shipping costs but will enable a new capability of unit level customization. Products will be fabricated with the specific color and shape required. New applications of electronics will be enabled by the ability to fabricate devices with unique and geometrically complex shapes—a cell phone shaped to the cavity of the user's inner ear or wearable computing custom fit to a specific human anatomy. In fact, human augmentation will be possible with the mass customization of prosthetics or bio-implantable devices. Other high-value systems in the defense or aerospace industry will also benefit from this capability with UAVs or disposable satellites designed, fabricated, and commissioned with mission-specific features in days rather than years [9].

This paper begins by describing previous work in 3D printing of electronics—the recent culmination of which includes a 3D-printed component that was integrated in a university-based satellite successfully launched into low Earth orbit in November of 2013. This application serves to demonstrate the reliability of 3D-printed electronics as space provides a particularly harsh environment in terms of thermal cycling, outgassing, and radiation. Although the device was functional during space qualification testing, several deficiencies were identified including (1) poor conductor performance

with the printed silver-based conductive inks serving as interconnect and (2) a lack of durability caused by the photopolymer resin used in the stereolithography-based dielectric substrate [10] that has an effect on outdoor weathering, heat aging, dimensional changes, color stability, and UV exposure behavior—a few characteristics used to evaluate durability of plastics by ASTM International. Consequently, a machine with a novel integration of technologies (described in section 3) has been developed and is referred to as the multi^{3D} system, which denotes the use of multiple technologies to produce 3D, multi-material, multifunctional devices. The multi^{3D} system produces parts with substantially improved mechanical, thermal, and electrical properties. The AM technology used for this multi^{3D} system is fused deposition modeling (FDM), a material extrusion AM process, which fabricates structures using more resilient thermoplastic materials but lacks the minimum feature size and surface finish necessary to create high-density and high-performance electronics. Moreover, the density of FDM-built parts precludes the use of conductive inks directly as electrical shorts are caused by the spreading of inks on surface layers and across stacked layers due to the inherent substrate porosity. However, by optimizing the FDM process and introducing micromachining and laser ablation capabilities, FDM can fabricate structures that are well suited to 3D electronics by providing substrates with enhanced dielectric and mechanical properties while simultaneously providing the required dimensional accuracies. An additional benefit of thermoplastics, as opposed to thermosetting photopolymers that do not remelt, is the ability to thermally embed solid wire conductors into the substrate without affecting planarization. Consequently, wires can now be seamlessly integrated and therefore minimize or eliminate the use of conductive inks as interconnect. Inks have significantly lower conductivity than bulk materials given the constraints of curing (temperature, outgassing of embedded traces, etc.). The system described within this paper includes all of these technologies and techniques, some of which are demonstrated here and some of which are the focus of future work, to enable an unprecedented capability to manufacture 3D structural electronics.

2 Previous work

Since the inception of the additive manufacturing industry, researchers have been investigating the technology in terms of fabricating end use products [11] and including embedded components [12]. An increasingly large number of researchers have shown interest in the specific capability of fabricating 3D and conformal electronics using AM, and reports are found as early as 1998 [13, 14]. The combination of direct printing (DP) of conductive inks onto solid freeform fabricated structures was introduced by Palmer et al. [15] and Medina et al.

[16, 17], in which modest circuits were implemented to demonstrate functionality by integrating a dispensing system into a stereolithography (SL) machine using 3D linear stages with a dispensing head. Lopes et al. [18] demonstrated a simple prototype temperature sensor with nine components including an integrated circuit in low-pin-density package, and in the same fashion, Palmer et al. demonstrated the fabrication of a prototype relay and electrical junction box by interrupting the SL process [2, 19]. Others have demonstrated a similar circuit as well as several clever electromechanical applications all created by an open-source fabrication system [20–22]. Navarrete et al. [23] described improvements to conductor density by introducing channels into the SL substrate for containing the conductive material in order to reduce the possibility of line-to-line shorting and improve the cross-sectional area for improved performance. Line spacing was thus controlled by the precision of the SL laser beam as opposed to the dispensing system. Additionally, this demonstration included not only digital logic and control but also radio frequency (RF) wireless functionality (e.g., antenna). The system was implemented in the form of a hidden-in-plain site rock to highlight the possibility of fabricating a line of systems—each of which could be altered in CAD to provide unique form similar to a snowflake and aiding in the deception by providing irregularities among the sensor systems. Ram et al. [24] reported electronics embedded in 3D-printed metal structures. More recently, collaborative work performed by Stratasys and Optomec reported the use of FDM with aerosol-sprayed conductors but used large pin pitch packaging [25, 26]. Most of the reported circuits to date required only the use of a single plane of routing (i.e., no interconnect crossover), although the concept of multiple planes with vertical interconnect was obvious.

With regard to introducing electrical interconnect at low temperature, Chrisey and Pique [27] and Pique et al. [28] described a technique referred to as laser-induced forward transfer (LIFT) that allows for the deposition of very thin lines in a variety of materials including copper with high resolution but limited to 2D applications. Substantial advancements in micro-dispensing of conductive ink resulted from a DARPA program in the early 2000s [29], and there has been significant effort in attempting to improve the conductive inks in general [30–33]. However, conductivity remains a major challenge not only for 3D-printed electronics but in the more general field of 2D-printed electronics as the inks typically provide poor conductivity if the substrate material (e.g., paper, cardboard, polymers, Kapton®) limits the temperature of subsequent curing.

Figure 1 illustrates three of four generations of a 3D magnetometer system with off-axis component placement and conducting routing, which included a microprocessor, LEDs, a DC connector, and three orthogonally placed magnetic Hall effect sensors [34]. Not only did these generations of magnetic sensor systems become successively

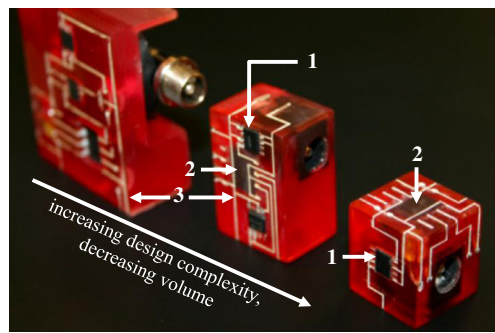


Fig. 1 First three generations of a three-axis magnetic flux sensor system using stereolithography, 1 Hall effect sensors, 2 microcontroller, and 3 conductive ink interconnect (image courtesy of Emerald Group Publishing Limited)

smaller but also demonstrated the progressive improvement of volume utilization—taking full advantage of the design in all three dimensions. However, each was fabricated with components placed on completely flat orthogonal surfaces. A fourth generation magnetic flux system [35] was fabricated with a cylindrical shape, demonstrating component placement and interconnect on curved surfaces as shown in Fig. 2. Moreover, the components employed were contained within modern surface mount packaging, providing smaller volume and higher density of pin placement. The previous generations of the magnetometer—as well as all other 3D-printed electronics using packaged silicon—have all been confined to through-hole components, which are used generally in hobbyist electronics or for prototypes using breadboards. By virtue of demonstrating surface mount technology, the electronics made possible by 3D printing now employ components that are akin to those

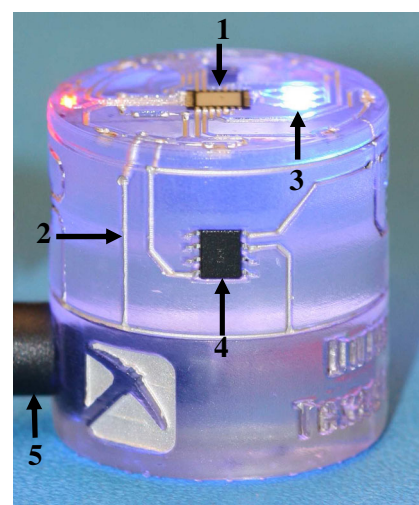


Fig. 2 Fourth generation of magnetic flux sensor system with curved surfaces and modern miniaturized electronic components (surface mount), 1 microcontroller, 2 conductive ink interconnect, 3 LEDs, 4 Hall effect sensors, and 5 power supply plug/connector

used in contemporary cell phones. Traditional printed circuit board CAD was used to create the wiring layout in 2D and was subsequently *deformed* with mechanical engineering CAD software (SolidWorks®) in order to create the final forms and 3D diagrams necessary to create the input files for stereolithography and micro-dispensing.

In other work, FDM processing parameters were developed for extruding and depositing low-melting-temperature metal alloys to produce a circuit pattern [36]. Although the work demonstrated the consistent deposition of a conductive metal (solder), the line widths were in the millimeter range and are considered too large to meet high-density electronics requirements. Although research may improve line widths using this approach, the physical limitations of the thermal extrusion process using solders will undoubtedly have challenges achieving densities required for microelectronics. Recent reports have also been published that indicate the preliminary use of FDM for the dielectric substrate along with aerosol spray for the implementation of interconnect [25]. Aerosol dispensing techniques provide ink-based conductors with high densities (20 μm line widths) and are well suited for conformal or nonplanar surfaces. FDM meanwhile provides a significantly better polymer base in terms of durability but at the expense of surface finish and minimum dimensional feature size. The FDM process—as used commercially—does not provide sufficient spatial resolution to fabricate sophisticated electronics, and furthermore, the aerosol conductors cannot be directly sprayed onto FDM forms as the porosity of stock fabrication can lead to shorts between electric lines. The team reporting this hybrid technology alleviated the shorting problem by cleverly spraying a dielectric ink to eliminate contact to the porous substrate. Of course, the additional step precludes the use of channels in the 3D-printed surfaces—often used to contain the inks, improve routing density, and provide an increased cross-sectional conductor area to improve conductance. The use of a dielectric ink mitigates the use of channels, and this may be viewed as an advantage; however, dispensing inks directly on the surface (without channels) will preclude continuing the build to produce fully embedded and optimized structures because the ink will either obstruct the FDM extrusion nozzle or the non-cured ink will be susceptible to damage by the traversing FDM extrusion nozzle. Also, the use of the dielectric ink may introduce adhesion or bonding issues with subsequent layers if full embedding is of interest. Dispensing inks into channels, on the other hand, mitigates these problems and allows the full embedding of components and interconnect. Conformally spraying the dielectric ink onto the bottom and sidewalls of the conductor channels would limit the miniaturization of these channels. Given that aerosol sprays provide very thin layers of conductors, conductivity of the printed lines will be a problem for high-power and high-frequency applications—particularly with the reduced curing temperatures dictated by

the maximum temperature of the thermoplastics. There is, however, ongoing work on laser curing [1, 37] and other directed energy methods such as broadcast photonic curing [38] for processing the inks without affecting the thermoplastic substrate.

2.1 Demonstration: CubeSat subsystem fabricated by using stereolithography and conductive inks

Based on the invitation to 3D print a subsystem of the Trailblazer CubeSat [39] (launched in November 2013) from Kirtland Air Force Base and the University of New Mexico's COSMIAC center, a design was created with a number of sensors and printed experiments that would help validate the use of 3D printing in the harsh environment of space as described in Lyke [9]. At the time of the original design, stereolithography had been demonstrated multiple times with dense volumetrically efficient 3D electronics and consequently chosen for fabrication of the design. A two-axis gyroscope was included along with a simple IIC-based SPA-1 interface to communicate to the satellite computer. Data collected from the sensors were formatted and transmitted every minute in order to prove continuous system functionality in low Earth orbit. Furthermore, although some data have been reported on the outgassing performance of 3D printing materials by NASA [40], a serpentine conductor was printed on the back-side of the structure—the resistance of which was intended to be determined based on a measured voltage to understand the impact of space conditions on printed conductors in terms of outgassing and thermal cycling. Figure 3 illustrates the component with backlighting to highlight the conductors on more than a single plane. Surface mount chips appear opaque and the four connections at the bottom provide strain-relieved electrical interfaces for the satellite computer. The connections include clock, data, and power rails. Mechanical connection was made through bolt holes as shown on the top left and

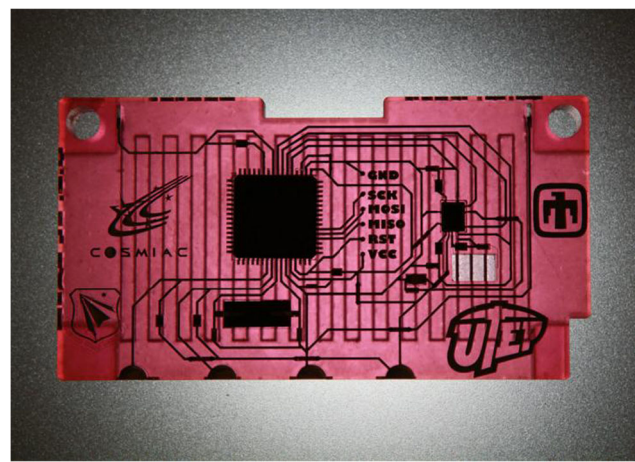


Fig. 3 Back illumination of CubeSat 3D-printed module produced by using stereolithography and direct print technologies

right. Although the form did not exploit the 3D freedom of AM, the volume used was dictated by the available space based on the remaining components in the CubeSat—most of which were confined to traditional fabrication—and thus limited the creativity of the subsystem form. Since the typical CubeSat geometries (i.e., square or rectangular prisms) are constrained by the Poly Picosatellite Orbital Deployer (P-POD), which interfaces between the CubeSat and the launch vehicle, the dimensions of the modules within the CubeSat are therefore constrained to planar geometries [41]. Potentially, 3D printing can completely open up the overall design of future deployers and CubeSats.

With regard to the serpentine conductor, experiments consisted of a long interconnect to provide a long printed ink trace susceptible to electrical discontinuity and the serpentine design occupied a majority of the available space on the bottom plane of the module to maximize the resistance and simplify measurement. To detect a discontinuity or degradation in continuity, a voltage divider circuit was designed and implemented using the serpentine as one of the resistors as a counter part to a fixed nonprinted resistor. Additionally, based on the measured voltage, a calculation can be performed to determine the actual resistance of the printed structure. Output from the CubeSat subsystem, which was within the 18 bytes per minute allowance, included an amplified ($4\times$ at a sensitivity of $2\text{ mV}^{\circ}/\text{s}$ and range of $\pm 2,000^{\circ}/\text{s}$) and unamplified measurement of angular rate from the gyroscope's pitch and roll, serpentine voltage as well as a variable that is periodically incremented from the point that the CubeSat subsystem is energized. This variable provides a value that changes monotonically as proof of system functionality if sensor data are stable and not changing. In combination, the electronic components were within the maximum power allowance of 300 mW.

In the final analysis, the stereolithography and conductive ink hybrid fabrication passed all dress rehearsal testings on Earth prior to launch and will be sufficiently durable to withstand a month-long mission in low Earth orbit. Even though using SL and conductive inks in combination enables the arbitrary placement of electronic component to produce 3D circuits, exploring other processes that may prove more reliable and offer production grade polymers is of interest. For example, an alternative to stereolithography materials, which are prone to failure in applications requiring long life given the sensitivity to prolonged UV exposure [10], is needed. In addition, conductive inks, which are perfectly reasonable for inventory-tracking circuits on cardboard boxes in retail stores, are limited in terms of conductivity and current carrying capacity. Both of these characteristics, conductivity and current carrying capacity, are not only affected by resistivity but are also necessary for high-power and high-frequency applications. As such, a robust conductor is unavoidable. In comparison to bulk copper (resistivity of $1.75\ \mu\Omega\text{ cm}$ [42]), copper

inks cured at $150\ ^\circ\text{C}$ have been reported as having a resistivity of $200\ \mu\Omega\text{ cm}$ [43], which is 2 orders of magnitude higher than its bulk counterpart. Although lower resistivities have been reported ($4.1\ \mu\Omega\text{ cm}$ for a copper nano ink annealed at $400\ ^\circ\text{C}$ for 60 min [44]), the annealing temperatures required to achieve these results are not suitable for 3D electronics due to the limitations imposed by the electronic components and substrate materials. These limitations and areas of interest have required and led to several novel breakthroughs in the fabrication of electronic-appropriate dielectric substrates as well as the integration of high-density, high-performance conductors within these dielectric structures as described in the next section.

3 Novel 3D printing of electronics

Several simultaneous fabrication capabilities are necessary in order to manufacture a diverse variety of 3D electronics systems—most but not all of which are provided by either multi-technology stereolithography or FDM platforms that include robotic placement of components and dispensing for ink conductors or embedding of solid conductors. Table 1 compares and contrasts three potential 3D printing implementations. The materials appearing in the table were selected after surveying the material properties found in the Wohlers report [45] to identify the top performers for the criteria of interest. The following discusses the comparison and lists the requirements and characteristics of 3D structural electronics.

1. The fabricated dielectric substrates require *high-performance electrical, thermal, and mechanical properties*. Thermoplastics are well known to be mechanically superior as highlighted in Table 1, in which ULTEM's Izod impact resistance is approximately an order of magnitude greater than that of the photocurable resins. With regard to thermal properties, polyphenylsulfone (PPSF) has a glass transition temperature that is 110 % greater than that of the Accura® Peak™ and a heat deflection temperature that is 24 % greater. In terms of electrical performance, although ULTEM and PPSF do not show an advantage over ProtoTherm 12120 when considering dielectric strength, there are advantages to using thermoplastics when considering dielectric loss. Vat photopolymerization relies on lossy photocurable resins, and augmenting these materials with fillers to achieve specific or enhanced electromagnetic properties is limited severely by chemistry and light scattering issues [46]. While laser sintering uses thermoplastics, the introduction of complementary technologies such as direct print poses many challenges due to the required inert nitrogen atmosphere and the base powder material. Alternatively, FDM systems are easier to modify

Table 1 System comparisons

		Vat photopolymerization		FDM		multi ^{3D} system	
		Somos ProtoTherm 12120 UV postcured	Accura PEAK UV and thermal postcured	ULTEM 9085	PPSF	ULTEM 9085	PPSF
Thermal	Glass transition temperature (°C)	74	110	186	230	186	230
	Heat deflection (°C) (ASTM D648 @ 0.46 MPa)	56.5	153	153	189	153	189
Mechanical	Tensile strength (MPa) (ASTM D638)	70.2	57–78	71.6	55	71.6	55
	Tensile elongation at break (%) (ASTM D638)	4	1.3–2.5	6	3	6	3
	Izod impact notched (J/m) (ASTM D256A)	12	21.3–27.3	106	58.7	106	58.7
Electrical	Dielectric strength (kV/mm)	15.5 (ASTM D149-97A)	Not available	11.4–4.33 (ASTM D149-09A)	11.4–3.1 (ASTM D149-09A)	11.4–4.33 (ASTM D149-09A)	11.4–3.1 (ASTM D149-09A)
	Spatial resolution (μm)	75 (laser diameter)	75 (laser diameter)	254 (nozzle orifice diameter)	254 (nozzle orifice diameter)	90 (laser micromachining results from Knowles et al. [48])	90 (laser micromachining results from Knowles et al. [48])

Source: Wohlers Report 2013 and manufacturer datasheets

and have a wider range of material options including those that have been successfully extruded like Zeonex® RS420, a thermoplastic with an electrical loss tangent similar to Teflon® [47]—2 orders of magnitude better than any SL resin. Thermoplastics can also be modified or enhanced with greater ease than photopolymers. This will enable the next generation of high-performance 3D antennas and other radio frequency applications.

- Given the tight dimensional requirements of electronic components including pin pitch and miniaturized package volume, the dielectric fabrication technology must provide *high spatial resolution* for the substrate. Whereas stereolithography has sufficient spatial resolution given the small beam width of the laser (~75 μm diameter in high-resolution mode of the SLA Viper si2 system), FDM produces feature sizes at or larger than 254 μm and is not natively appropriate for electronics fabrication. For example, with a 0.65-mm pitch 144-pin TQFP package common in contemporary electronics, the chip cavity requires a flush encapsulation with pin features including 450-μm openings with 200-μm separation fins—to provide mechanical support and electrical access to the packaged

silicon. Therefore, to provide the feature resolution necessary in the context of FDM fabrication, the multi^{3D} system implements additional high-resolution subtractive methods (i.e., CNC micromachining demonstrated by the current system and laser ablation for a future system to achieve channel widths of ~100 μm and even smaller). In related research, Knowles et al. demonstrated through optical images ~90-μm feature resolution using a laser ablation approach with a polyimide substrate [48].

- When conductive inks are still appropriate (i.e., no high-current-density requirements and the simultaneous need for the spatial freedom provided by micro-dispensing), the dielectric substrate must have *superior surface finish with minimal porosity*—otherwise, the porosity will result in shorts between electrical lines as the conductive inks will spread prior to curing. Consequently, the multi^{3D} system includes FDM build parameter optimizations (e.g., raster to raster air gap, raster width) for printing with improved density to maintain separation of conductive ink traces.
- In cases where the interconnect is required to provide *high current densities with bulk level conductivity* (1.68e-8 Ω m as a reference), wires can be introduced providing

performance which is impossible to achieve with cured conductive inks (or even the solder-based approach described previously). In the multi^{3D} system, wires are embedded with a novel patent-pending thermal embedding technique [7, 8] that submerges wires as small as 80 µm in diameter firmly into the thermoplastic substrates fabricated with FDM—leaving a planar surface to continue the interrupted fabrication process.

The developed multi^{3D} system is shown in Fig. 4 (left) and illustrates how two FDM machines can be integrated together, sharing a sliding platform and where a middle compartment is included for micromachining, component placement, ink dispensing, and embedding of wires—or any other required technology necessary to augment the capabilities of the part being built. Figure 4 (right) shows a conceptual model of a potential fabrication—wherein a variety of dielectric materials can be placed with full 3D freedom. Furthermore, modern electronic components and sensors as well as the high-performance interconnect can be embedded during process interruptions as shown in the center of the image.

The current state of the multi^{3D} system includes two legacy FDM machines connected via a pneumatic slide that enables the fabrication of multi-material parts [49, 50]. Additionally, a CNC router and precision dispensing system have been incorporated to enable micromachining of interconnect channels and component cavities as well as dispensing of conductive inks. These technologies are controlled by using a custom-made program developed using LabVIEW to provide automation and seamless manufacturing between the different technologies.

The motivation for using embedded wires is driven from the excessively high resistances resulting from the use of conductive inks compounded by the limit on ink curing temperature imposed by the polymer substrate and embedded electronic components. In addition, the malleability offered by copper wires that is needed for surviving dynamic mechanical loading is beneficial in terms of flex performance. High resistances cause self-heating, conductor voltage drop and both reduced reliability and performance. To illustrate this

limitation, Table 2 shows the calculated resistivity and resistance for a benchmark (standard PCB manufacturing) at 10 cm of length. For comparison, values are reported for inks, extruded solder, and embedded wires. The resistivity allows for a direct comparison (i.e., independent of geometry) between the conductors, but from an applications standpoint, the resistance was considered as it reflects the standard geometric configurations found in manufacturing. In either case, inks were found to have a higher resistivity and resistance when compared to the benchmark or embedded wires. For the benchmark PCB, 37 µm is the standard thickness for 1-oz copper and 4 mils (~100 µm) is a representative trace width for an economical technology. Alternatively, inks are generally quoted with sheet resistance values for a 1.0-mil thickness (~25 µm), but the printed traces can be thinner for any micro-dispensing technology (including ink jetting, aerosol jetting, syringe fluid dispensing, etc.), which only results in further reductions in the conductivity. In the case of screen-printing or micro-dispensing, the thickness can be increased with careful process engineering and generally at the expense of routing density due to limits on aspect ratios. However, for this study, a thickness of 1 mil was considered reasonable and conservative for comparison purposes. For the method under development, three wire gauges were used: 40 gauge (~80 µm diameter), 32 gauge (~200 µm diameter), and 28 gauge (~320 µm diameter)—all three of which have been successfully embedded into FDM substrates. From the table, embedded 40 gauge wires are equivalent to PCBs in terms of resistance. Furthermore, at this gauge, the circuit density can meet or exceed that of the PCB (80 µm diameter versus 100 µm width). Only in the case of state-of-the-art PCB technology (2 mil or 50 µm widths) would the multi^{3D} system fail to compare in terms of density—which may necessitate the use of conductive inks for a small fraction of dense routing.

For the conductive inks, the resistance was calculated based on resistivity reported in the manufacturer's datasheets [51, 52]. Some improvement may be possible through the use of location-specific methods such as laser or ohmic curing [1, 53], but in all cases, although bulk conductivity is approached, an unavoidable penalty remains for inks. The increased

Fig. 4 The multi^{3D} system (*left*) and schematic of fabrication example (*right*)

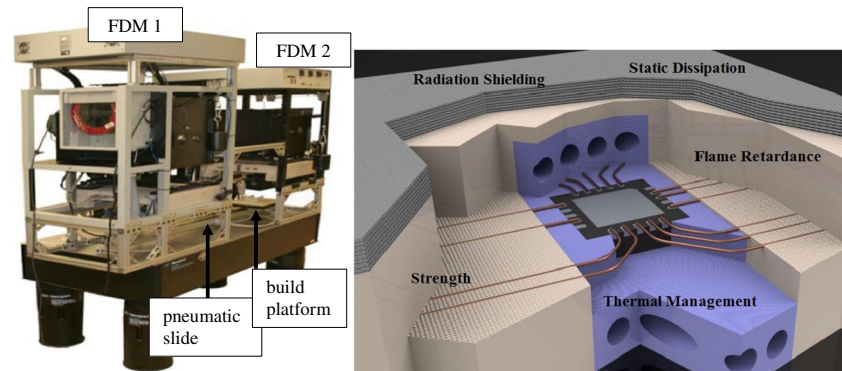


Table 2 Comparison of resistivity and resistance for select conductors

Case	Geometry	Resistivity ($\Omega \text{ m}$)	Resistance (Ω)
1 oz copper PCB with 4 mil width	37 μm thick, 100 μm wide, conductor 10 cm long	1.7×10^{-8}	0.45
Dupont Ink CB028 Silver	25 μm thick, 100 μm wide, conductor 10 cm long	11.8×10^{-8}	4.73
Dupont Ink CB500 Copper	25 μm thick, 100 μm wide, conductor 10 cm long	50.7×10^{-8}	20.27
Extruded solder	25 μm thick, 100 μm wide, conductor 10 cm long	7.2×10^{-8}	2.86
40 gauge wire 10 cm long	80 μm diameter, conductor 10 cm long	1.7×10^{-8}	0.33
32 gauge wire 10 cm long	200 μm diameter, conductor 10 cm long	1.7×10^{-8}	0.05
28 gauge wire 10 cm long	320 μm diameter, conductor 10 cm long	1.7×10^{-8}	0.02

resistance of inks—although limiting performance, resulting in excess heating, and potentially reducing system reliability—may be acceptable in a limited number of low power, low performance applications. From this standpoint, the capability of dispensing inks is included in the multi^{3D} system in order to provide additional manufacturing flexibility such as printing directly to silicon die where feature sizes do not allow for laser welding or to fill crossover tunnels with conductive material. When dispensed into 3D-printed channels, resistances can be mitigated through increased cross-sectional area without the need for high-aspect-ratio printing. Furthermore, channels—introduced in Navarrete et al. [23]—allow the 3D printing technology to dictate line separation—allowing the dielectric deposition process to dictate routing density through line pitch rather than the direct-write process with the potential for ink spreading. The main challenge with channels is that any porosity within the substrate may lead to shorting without first applying a dielectric layer prior to the conductor printing or, as is done in this work, optimizing the FDM process to remove undesirable porosities.

Obviously, as functionality in terms of hardware is added to the system, the cost increases. The required software for process planning and hardware control of this experimental system is not clearly known, but it is anticipated that this software will be the same for all versions of the multi^{3D} system and therefore identical in cost regardless of the system's functionality. Since the existing system is experimental, the system has not been designed or optimized for commercialization. As a result, the cost of a specific commercial system is not known. However, it should be noted that this system has been designed as a modular system that enables adding functionality at incremental cost. For example, a base system—which is anticipated to include two FDM machines and a CNC micromachining system—could be purchased with the additional capabilities of ultrasonic welding for the additional cost of the ultrasonic welding equipment. Thus, a variety of systems could be sold, employing different technologies for specific fabrication needs. Furthermore, a service provider could house a single or multiple “extraordinarily capable” system(s) for contract manufacturing of custom components in a foundry-type environment.

4 Methodology for manufacturing using the multi^{3D} system

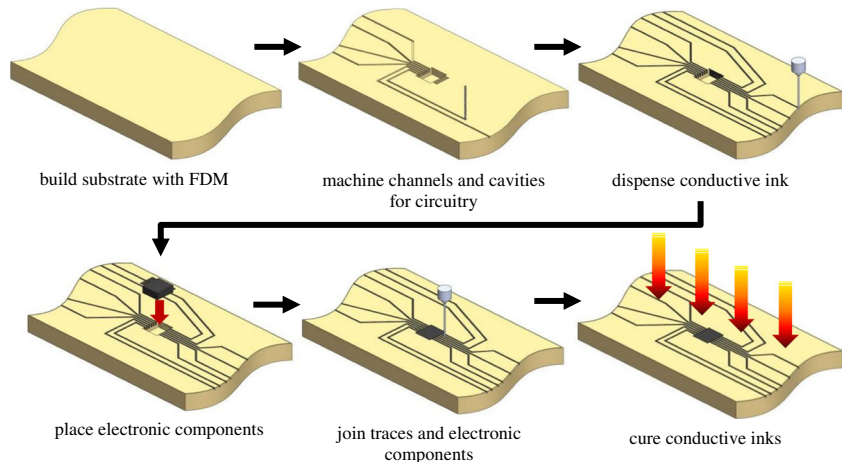
With these electronic fabrications in mind, a manufacturing platform has been developed that integrates two FDM systems, a CNC router for micromachining and a precision dispenser for depositing conductive inks. Future efforts will demonstrate the automated process for fabricating 3D electronics with this system, but the work presented here demonstrates only a fraction of the capabilities of the multi^{3D} system. The following sections describe (1) the fabrication of the CubeSat Subsystem presented in section 2 except using FDM, micromachining, and precise dispensing and (2) the ongoing work of embedding copper wire conductors into FDM-fabricated substrates.

4.1 CubeSat subsystem fabricated by using FDM and conductive inks

The process steps (shown in Fig. 5) required for producing the FDM-built CubeSat modules consisted of (1) fabricating the blank substrates using FDM, (2) micromachining the interconnect and component cavity features using a CNC router, (3) depositing conductive ink using a custom-built automated ink dispensing system, (4) manually populating component cavities with the respective component (although robotic component placement is being investigated), and (5) thermally curing the ink. Additionally, an attempt at building the complete CubeSat module (including microscale features) was made by using the FDM machine to demonstrate the need for micromachining. The term microscale is used here, but it should be noted that features in the range of 50 to 5,000 μm are produced by conventional mesoscale machining.

As mentioned earlier, the substrate material should exhibit high-performance electrical properties and as such FDM materials were compared to Kapton (a flexible dielectric substrate) [54] and FR-4 (a glass-reinforced epoxy used for printed circuit boards) [55]. As shown in Table 3, ULTEM 9085 has a similar volume resistivity, dielectric constant, and dissipation factor as that of Kapton and FR-4. For the fabrication of the CubeSat module, ULTEM 9085 was chosen over

Fig. 5 Process steps for producing the 3D-printed CubeSat module using FDM and conductive inks



other FDM materials since its UL94 flame classification of V-0 is the highest (i.e., most flame retardant) among that group of materials. In similar work, ULTEM was used as a substrate, which was laser micromachined to produce pockets for electronic components that were ultimately embedded [28]. Interconnect pockets were also micromachined for containing a conductive paste that were deposited using laser direct write. In that work, ULTEM was selected due to its thermal and mechanical stability, which was required during thermal curing cycles performed on the conductive pastes.

After fabricating the blank ULTEM substrates, the top and bottom surfaces of each individual part was micromachined using a tabletop CNC router (model LC 3024, Techno, Inc., New Hyde Park, NY, USA) to produce the component cavities and interconnect channels. The router was equipped with an automatic tool changer and has been reported as having a 5.08- μm (0.0002 in.) resolution and 25.4- μm (0.001 in.) repeatability www.technocnc.com. The spindle speeds and feed rates were calculated using data (i.e., cutting speed constants and feed per tooth) for polycarbonate due to the available data [56], and the standard machining formulas were used [57]:

$$\text{spindle Speed (revolutions per minute)} = \frac{\text{cutting speed constant} \times 4}{\text{cutter diameter (in.)}}$$

$$\text{feedrate (in.per minute)} = \text{feed per tooth (in.)} \times \text{spindle speed}$$

While the component cavities were simply machined to accommodate the component dimensions, the interconnect channels were machined to a depth of 0.127 mm (0.005 in.) or half the layer thickness. This cutting depth was determined through an empirical study, and this depth aided in eliminating the electrical shorting that was seen when using other cutting depths. Prior to machining the FDM CubeSat blank substrates, ULTEM substrates produced using select FDM parameters were machined to produce adjacent channels with a separation of 254 μm and depths of 127, 254, and 381 μm , which correspond to half a layer thickness, a full layer thickness, and one and a half layer thickness, respectively. After depositing and curing the ink in the machined channels, a stereomicroscope (Leica MZ16, Leica Microsystems Inc., Bannockburn, IL) equipped with a CCD camera (Retiga 2000R Fast 1394, QImaging Corp., Canada) was used to inspect the ink within the channels and identify areas where the ink spread. Additionally, the samples with channels and deposited ink were cut and polished to produce cross-section images for optical microscopy analysis.

Table 3 Electrical properties of select FDM materials, Kapton, and FR-4

	Volume resistivity (ASTM D257) ($\Omega \text{ cm}$)	Dielectric constant (ASTM D150)	Dissipation factor (ASTM D150)	Dielectric strength (ASTM D149) (V/mm)
PC ^a	2.0E+14–6.0E+13	3.0–2.8	0.0006–0.0005	360–80
ULTEM 9085 ^a	1.0E+14–6.0E+13	3.2–3.0	0.0027–0.0026	290–110
ABS-M30 ^a	4.0E+14–5.0E+13	2.9–2.7	0.0052–0.0049	370–71
PC-ABS ^a	2.0E+14–4.4E+13	2.9–2.7	0.0035–0.0032	340–90
Kapton ^b	1.0E+17	3.5	0.0026	154,000
FR-4 ^c	5.0E+12	4.6	0.015	–

^a Data from www.stratasys.com

^b Data from www2.dupont.com

^c Data for Shengyi S1141 from www.agssales.com/pcb-datasheets-shengyi.html

For the dispensing of conductive inks, an inexpensive (~US\$1,400), precision dispensing system (model Ultra 2400 Series, Nordson EFD, Westlake, OH) was fixed onto the CNC router and conductive inks were dispensed in an automated fashion. After the conductive ink (model 1660, Ercon Inc., Wareham, MA) was deposited, the insertion of each electronic component was performed manually. Subsequently, the conductive ink was cured by placing the CubeSat module in an oven at 60 °C for 60 min.

To compare the dimensional accuracy achieved by the FDM and CNC router machine, a substrate with rectangular and cylindrical cutouts was designed and manufactured using either FDM or CNC machining. The rectangular cutouts oriented with the *x*- and *y*-axes were spaced to produce walls of thicknesses 6.35, 5.08, 3.81, 2.54, 1.27, and 0.508 mm (0.25", 0.2", 0.15", 0.1", 0.05", 0.02") which represent separations between traces. Two separate sets of rectangular cutouts (one orientation with the *x*- and *y*-axis and the other rotated 45° from the positive *x*-axis) were produced, in which each cutout exhibited different widths: 6.35, 2.54, 1.27, and 0.508 mm (0.25", 0.1", 0.05", 0.02"). These features were included to determine the minimum width that can be produced by either method. The circular cutouts ($\varnothing=2.54$, 1.52, 1.02 mm) were included to represent through-hole or blind vias. For all features, the percent error was calculated using the CAD dimensions as the reference.

4.2 Embedding copper wire conductors into FDM-fabricated substrates

Although not fully mature, the work presented in this section demonstrates the use of copper wire conductors in combination with FDM. To secure the wire in the thermoplastic substrate, ultrasonic energy (20 kHz, 500 W power supply equipped with a 0.5" exponential horn modified to allow a wire to be fed along a central axis) was used to fully embed the wire such that the substrate remained planar, which allows subsequent thermoplastic deposition via FDM. In addition, a joule heating method (i.e., passing an electrical current through the wire sufficient to cause heating) was developed to heat the wire and enable an alternative method for full wire embedding. In separate experiments, a YAG laser microwelding system (model LW5AG, Miyachi Unitek, Monrovia, CA) was used to produce solderless joints between the wire and the electronic component.

5 Results and discussion

The FDM-built CubeSat module (including microscale features) lacked the feature details (see Fig. 6) required for the electronic component pins and interconnect channels and as such demonstrated the need for micromachining. The

micromachined substrates, on the other hand, contained well-defined component cavities and interconnect channels with consistent dimensions (channel width, $506\pm4\ \mu\text{m}$ based on five equally spaced measurement along a 20-mm distance; target value, 508 μm). Despite the machining of microscale features using small milling tools (end mills with $\varnothing=3.18$, 1.59, 1.27, 0.51, 0.41 mm (1/8", 1/16", 0.050", 0.020", and 0.016")), the total machining time was only 8 min for the top surface and 3 min for the bottom surface containing the serpentine.

In terms of accuracy, the percent error is reported in Fig. 7 for the rectangular and circular cutouts. For this analysis, a 1 % error was used as a baseline since 1 % is considered a "loose" tolerance for injection molding of ABS; however, some features may require tolerances as low as 0.25 % [58]. When oriented with the *x*- and *y*-axes, the width of the rectangular cutouts (Fig. 7a) exhibited an approximate 1 % error for widths 2 mm or greater, regardless of manufacturing method. For the rectangular cutouts oriented at 45° (Fig. 7b), CNC machining produced widths of 2 mm or greater within 1 % error; however, FDM could only produce the ~6 mm width for the same error. A notable difference was also seen for the wall thickness measurements (Fig. 7c)—within a 1 % error, FDM and CNC produced wall thicknesses of ≤ 4 mm. It should also be noted that even though the wall thicknesses produced using FDM and CNC machining exhibited similar percent error, the FDM-produced walls were not solid (i.e., the contours were accurately spaced apart but the material between the contours did not fill the inside of the walls completely). For the diameter ranges tested here (Fig. 7d), only CNC was able to produce circular cutouts within a 1 % error. Since the CNC machining steps add processing time, they should be used only when necessary. As such, the percent error for these rectangular and circular features can be used during the design stages to determine which technology should be used to produce interconnect channels (if required) and electronic component cavities.

The micromachining process resulted in an additional step; however, surface peaks and valleys inherent to the FDM process [59] were removed, which enabled, to a limited extent, the containment of ink and in some cases mitigated electrical shorting that has been noted in other work [25]. Figure 8 is a top view (XY plane) of the ULTEM substrates in which the topmost layer shows rasters oriented at 135° from the positive *x*-axis. Rasters oriented at 45° from the positive *x*-axis belong to the layer that was below the topmost layer. These images highlight the areas where ink spreading was observed beneath the top layer. The ink was not contained within the channels when the standard raster to raster air gap was used, and in fact, continuity tests confirmed the ink spread between the adjacent channels resulting in electrical shorting. Substrates fabricated with a -12.7 - and $-25.4\text{-}\mu\text{m}$ raster to raster air gap also exhibited ink spreading; however, with the

Fig. 6 Microscale features for the 3D-printed CubeSat module produced by FDM (*left*) and micromachining (*right*). Note that for all features, FDM was unable to produce the pin cavities (*top*), interconnect channels (*middle*), and pin/interconnect junction (*bottom*)

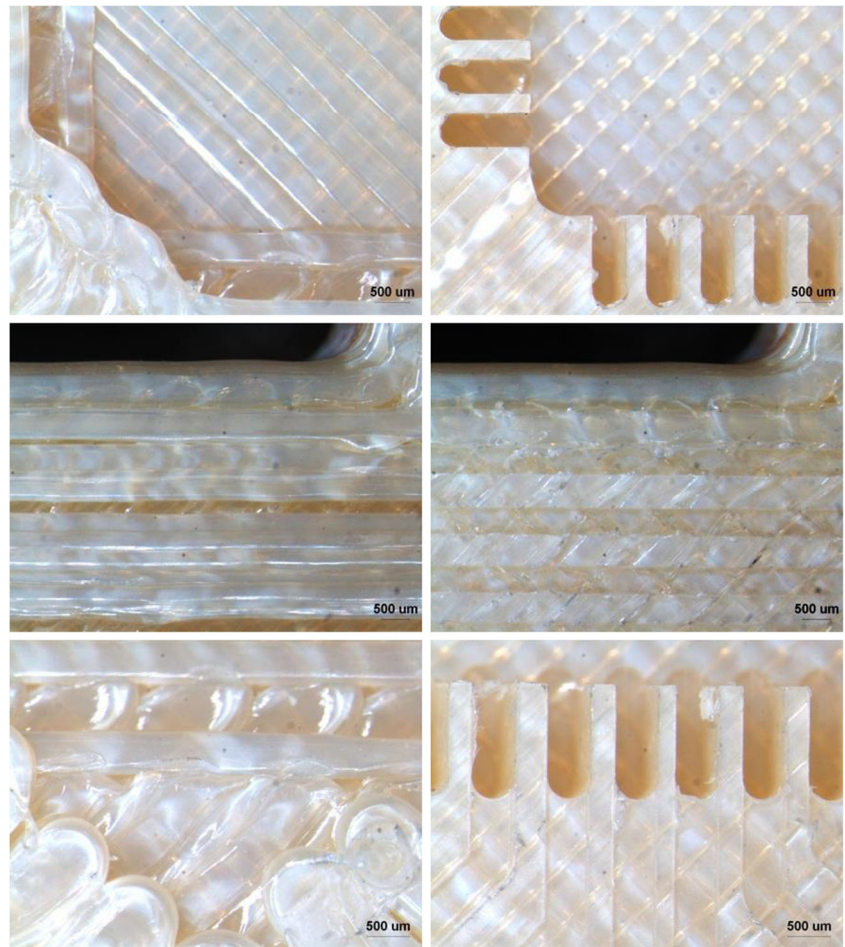


Fig. 7 Average dimensions of **a** width of rectangular cutouts oriented along x - and y -axes, **b** width of rectangular cutout oriented along a 45° from positive x -axis, **c** wall thickness between rectangular cutouts, and **d** circular cutout diameter. Note that the legend for the graph in **a** applies to the other graphs

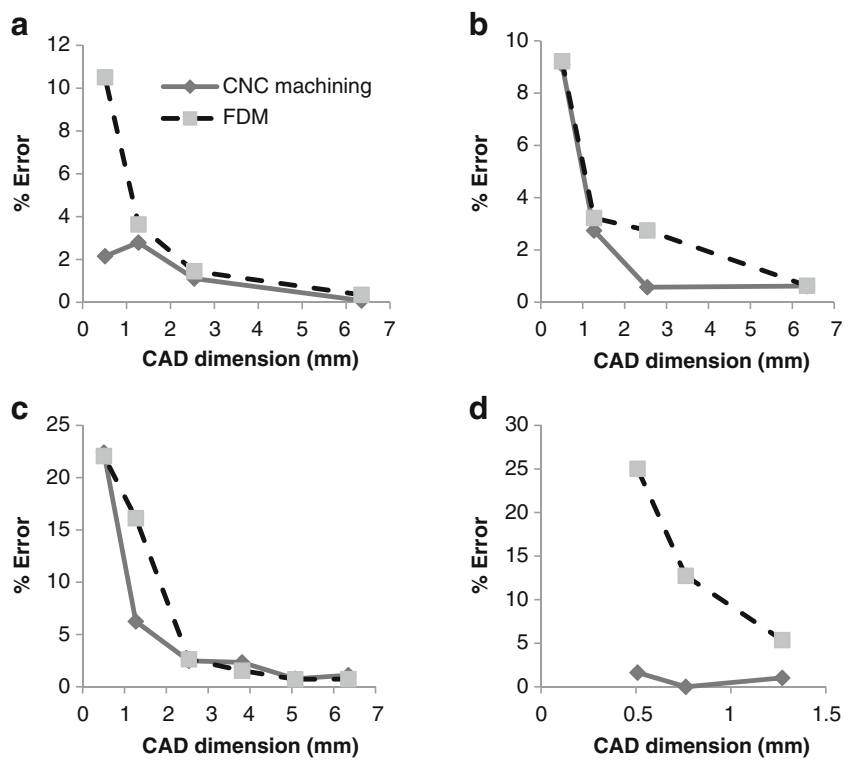
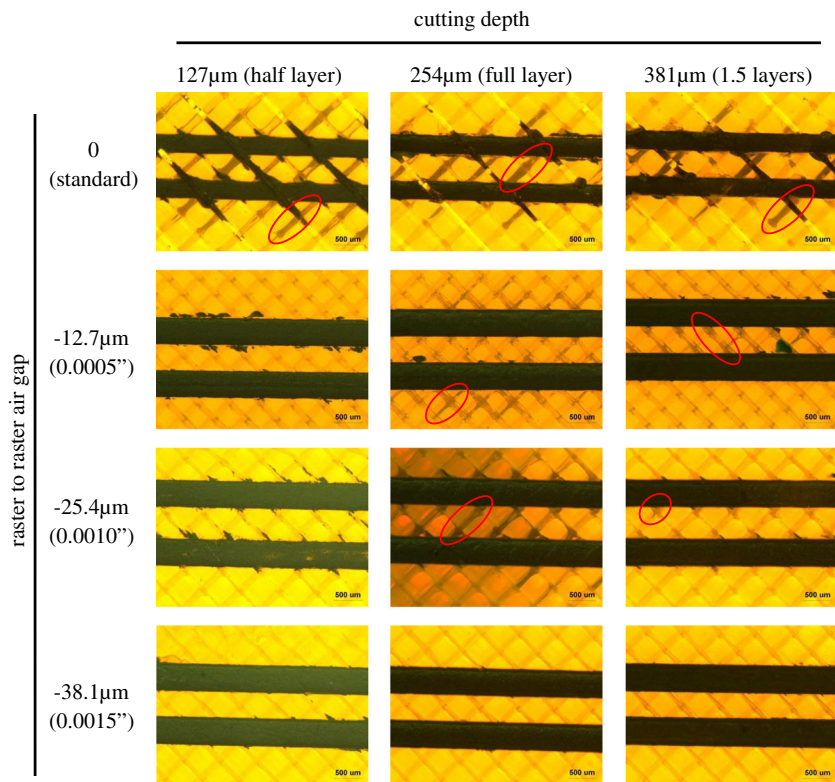


Fig. 8 ULTEM substrates built using different raster to raster air gaps (rows) and micromachined using different cutting depths (columns). Regions where inks have spread below the surface are circled



exception of one substrate ($-25.4\text{-}\mu\text{m}$ raster to raster air gap and cutting depth of $254\text{ }\mu\text{m}$), the interconnect did not electrically short. Evidence of ink spreading or containment was also confirmed using cross-sectioned specimens (Fig. 9). The

substrates fabricated with a $-38.1\text{-}\mu\text{m}$ raster to raster air gap yielded the best results in terms of containing the ink within the channel, and therefore the CubeSat module was fabricated using this air gap. For the particular geometry of the CubeSat

Fig. 9 Cross-sectional images of interconnect channels and cured ink. Features produced using **a** $-25.4\text{-}\mu\text{m}$ air gap and $254\text{-}\mu\text{m}$ cutting depth, **b** $-12.7\text{-}\mu\text{m}$ air gap and $254\text{-}\mu\text{m}$ cutting depth, **c** $-38.1\text{-}\mu\text{m}$ air gap and $127\text{-}\mu\text{m}$ cutting depth, and **d** $-38.1\text{-}\mu\text{m}$ air gap and $381\text{-}\mu\text{m}$ cutting depth. Note that ink not contained within the channels is highlighted by the arrows

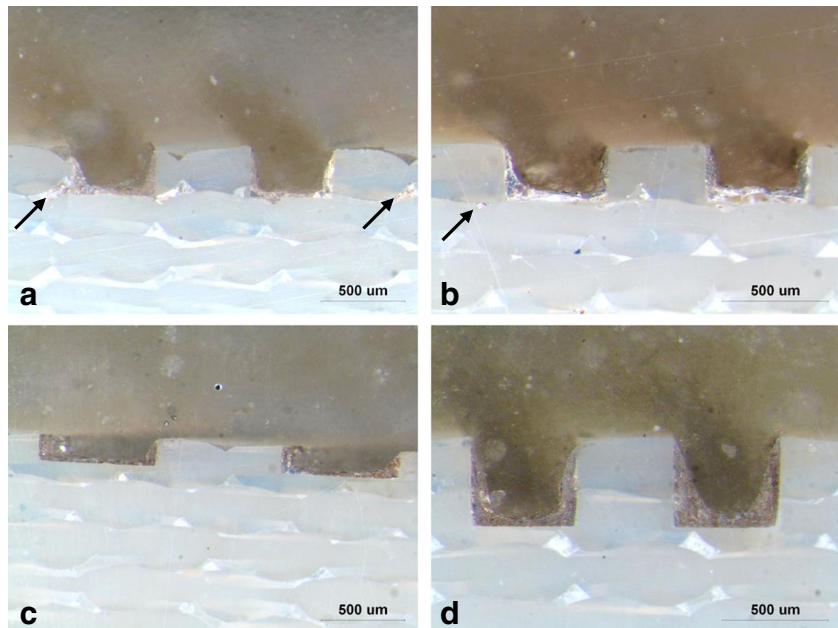


Fig. 10 3D-printed CubeSat module produced by using fused deposition modeling (substrate material is ULTEM 9085), CNC routing, and direct print technologies

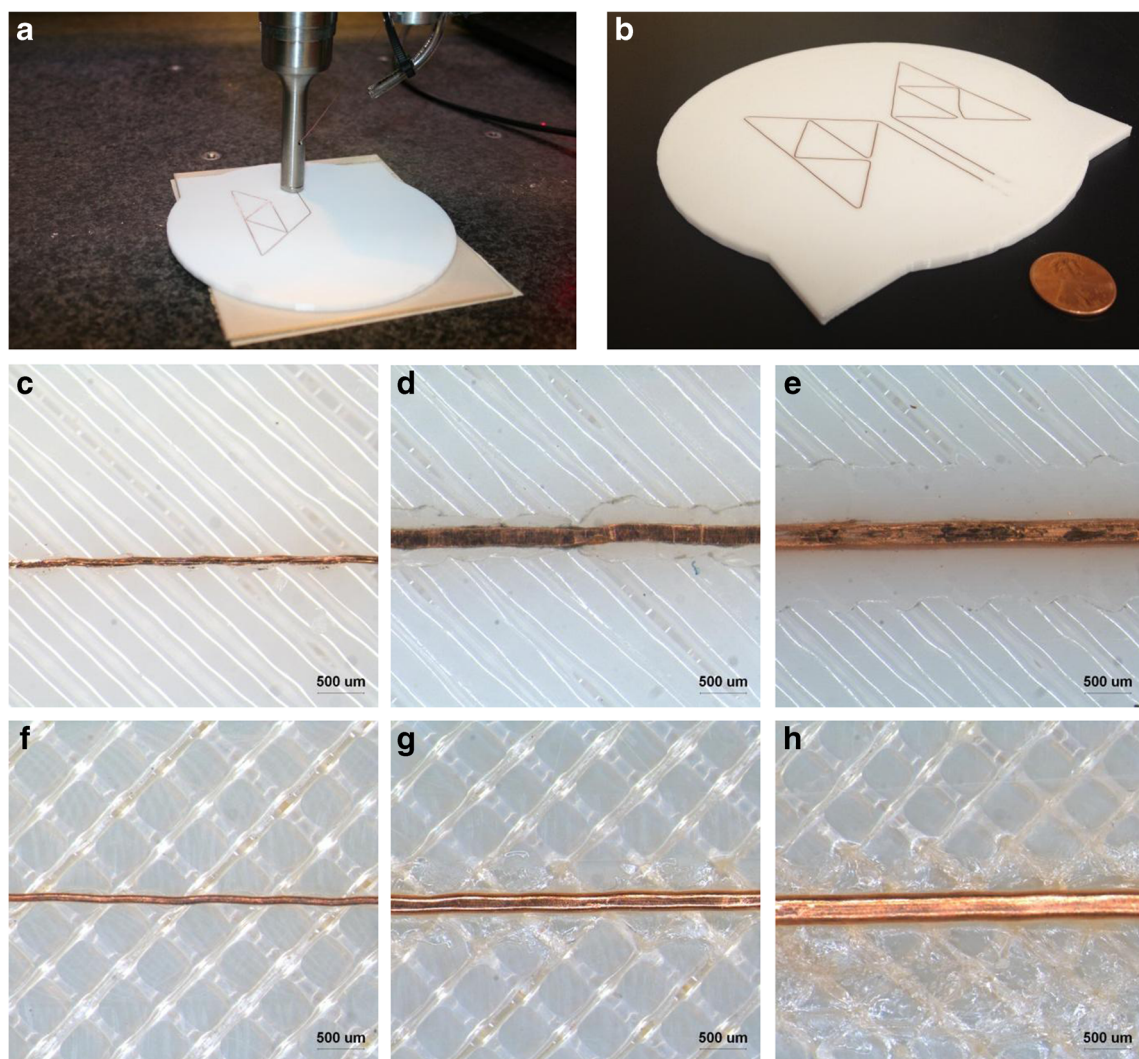
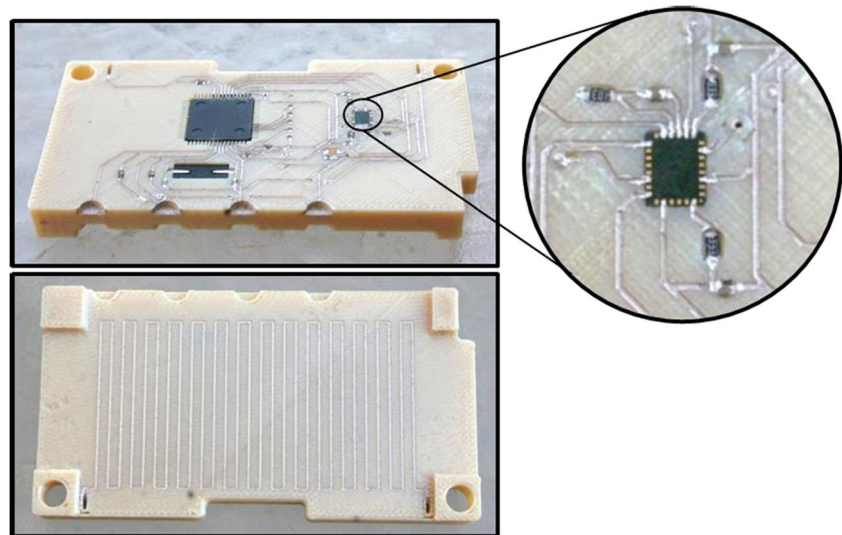
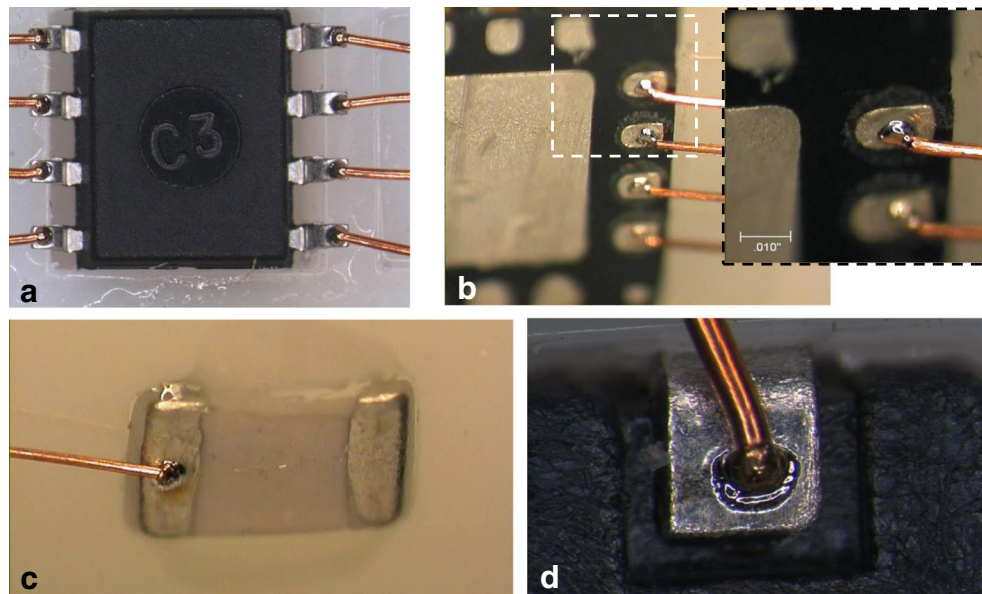


Fig. 11 Demonstration of embedded copper wires in ULTEM 9085 and polycarbonate (PC) substrates: **a** ultrasonic embedding setup, **b** antenna pattern on PC substrate, **c** 40 gauge copper wire in PC, **d** 32 gauge copper

wire in PC, **e** 28 gauge wire in PC, **f** 40 gauge copper wire in ULTEM, **g** 32 gauge copper wire in ULTEM, and **h** 28 gauge wire in ULTEM

Fig. 12 Laser-welded interconnect of various surface mount devices including **a** 555 timer IC, **b** MEMS accelerometer, **c** chip capacitor, and **d** crystal oscillator



module, the combination of raster width and air gap allowed the deposited thermoplastic to cover the entire area of each layer cross-section resulting in the absence of voids between adjacent rasters and therefore containing the ink within the channel. Additionally, since the cutting depth did not seem to have an effect on the ink spreading for the $-38.1\text{-}\mu\text{m}$ air gap specimen, a cutting depth of $127\ \mu\text{m}$ was used to reduce the amount of stress and wear on the micromachining cutters. The resulting CubeSat subsystem (top and bottom surfaces) is shown in Fig. 10.

Figure 11 shows an antenna pattern made of copper wire, which was embedded into polycarbonate in an automated fashion and may be used for low-profile planar antennas [60]. Ultimately, the ability to arbitrarily embed copper wire in three dimensions can enable many applications including, for example, the fabrication of functionally enhanced 3D antennas that can achieve improved gain or bandwidth, tailored to specific applications. The embedding process was also demonstrated by using various wire gauges and FDM materials as shown in Fig. 11c–h, in which ULTEM and polycarbonate substrates contain embedded copper wires. Note the presence of heat-affected zones adjacent to the embedded wire. These zones appeared to increase as the wire diameter increased and will be the focus of future work to determine the relation between the various processing parameters (e.g., ultrasonic amplitude, pressure applied to substrate, wire diameter, substrate material, surface roughness, traversing speed).

The joining of interconnect and electronic component is critical to the reliability of the device. Laser microwelding is proposed because this process is highly localized to minimize or eliminate damage to the substrate or electronic component and potentially can achieve welds that support high

interconnect densities. Figure 12 shows laser-welded joints, which were achieved without the use of filler metals or solders that can likely contaminate the electronic device or other subsequent manufacturing steps. When compared to soldering, laser welding produces stronger joints and smaller heat-affected zones. Also, a laser welding system may be easier to implement within the native FDM environment than would be a traditional reflow soldering system.

6 Conclusions

A manufacturing technology (multi^{3D} system) has been described that in a single build sequence provides a functional polymer substrate with sufficient density and spatial features to implement 3D-printed electronics for a wide range of applications including space electronics or biomedical devices. Process interruptions allow for the insertion of electronic devices and the conductors necessary to electrically interconnect the components. With FDM enhanced by complementary subtractive technologies (micromachining and laser ablation) and optimized for improved density, components can be connected either through conductive inks dispensed in channels or by high-performance, high-gauge wires embedded within the substrate and joined by using laser welding. A fraction of the capabilities provided by the multi^{3D} system were demonstrated through the fabrication of the CubeSat subsystem by using FDM and direct print technologies. As 3D printing only requires a modifiable CAD depiction of the electronic system to be printed, unit level customization can be enabled by this transformational technology—including human anatomy-specific biomedical devices or rapidly deployed mission-customized spacecraft.

Acknowledgments The research presented here was performed at The University of Texas at El Paso (UTEP) within the W.M. Keck Center for 3D Innovation (Keck Center), expanding recently to over 13,000 sq. ft. and providing access to state-of-the-art facilities and equipment as a result of funding, most recently, from the State of Texas Emerging Technology Fund. Support was provided, in part, by the University of Texas System Louis Stokes Alliance for Minority Participation Program under grant NSF-HRD-1139929 as well as the Mr. and Mrs. MacIntosh Murchison Chair I in Engineering Endowment. The authors are grateful for the assistance of Alfonso Fernandez, Jorge Ramirez, David Rodriguez, Lluvia Herrera, Rudy Salas, and Efrain Aguilera of the Keck Center on various aspects of the project. The authors are also grateful to Bob Zinniel of Stratasys for his assistance in adapting FDM capabilities to the multi3D system as well as Jim Lyke at Kirtland AFRL and Craig Kief at Cosmiac at the University of New Mexico for application guidance in satellite electronics.

References

- Lopes AJ, MacDonald E, Wicker RB (2012) Integrating stereolithography and direct print technologies for 3D structural electronics fabrication. *Rapid Prototyp J* 18:129–143. doi:[10.1108/13552541211212113](https://doi.org/10.1108/13552541211212113)
- Palmer JA, Jokiel B, Nordquist CD, Kast BA, Atwood CJ, Grant E, Livingston FJ, Medina F, Wicker RB (2006) Mesoscale RF relay enabled by integrated rapid manufacturing. *Rapid Prototyp J* 12:148–155. doi:[10.1108/13552540610670726](https://doi.org/10.1108/13552540610670726)
- Wicker R.B, Medina F, Elkins CJ (2004) “Multiple material micro-fabrication: extending stereolithography to tissue engineering and other novel applications,” *15th Annual Solid Freeform Fabrication Symposium*, University of Texas at Austin, August 2–4, 2004, pages 754–764
- Wicker RB, MacDonald EW (2012) Multi-material, multi-technology stereolithography. *Virtual Phys Prototyp* 7:181–194. doi:[10.1080/17452759.2012.721119](https://doi.org/10.1080/17452759.2012.721119)
- Gutierrez C, Salas R, Hernandez G, Muse D, Olivas R, MacDonald E, Irwin MD, Wicker RB, Church K, Newton M, Zufelt B (2011) CubeSat fabrication through additive manufacturing and micro-dispensing. *Proceedings from the International Microelectronics Assembly and Packaging Society Symposium*
- Castillo S, Muse D, Medina F, MacDonald E, Wicker R (2009) Electronics integration in conformal substrates fabricated with additive layered manufacturing. *Proceedings of the 20th Annual Solid Freeform Fabrication Symposium*. pp 730–737
- Wicker RB, Medina F, MacDonald E, Muse DW, Espalin D (2013a) Methods and systems for embedding filaments in 3D structures, structural components, and structural electronic, electromagnetic and electromechanical components/devices. Patent Pending
- Wicker RB, Medina F, MacDonald E, Muse DW, Espalin D (2013b) Methods and systems for connecting inter-layer conductors and components in 3D structures, structural components, and structural electronic electromagnetic and electromechanical components/devices. Patent Pending
- Lyke JC (2012) Plug-and-play satellites. *IEEE Spectr* 49:36–42. doi:[10.1109/MSPEC.2012.6247560](https://doi.org/10.1109/MSPEC.2012.6247560)
- Tröger C, Bens AT, Bermes G et al (2008) Ageing of acrylate-based resins for stereolithography: thermal and humidity ageing behaviour studies. *Rapid Prototyp J* 14:305–317. doi:[10.1108/13552540810907983](https://doi.org/10.1108/13552540810907983)
- Kruth J-P, Leu MC, Nakagawa T (1998) Progress in additive manufacturing and rapid prototyping. *CIRP Ann Manuf Technol* 47:525–540. doi:[10.1016/S0007-8506\(07\)63240-5](https://doi.org/10.1016/S0007-8506(07)63240-5)
- Kataria A, Rosen DW (2001) Building around inserts: methods for fabricating complex devices in stereolithography. *Rapid Prototyp J* 7:253–262. doi:[10.1108/13552540110410459](https://doi.org/10.1108/13552540110410459)
- Weiss L, Prinz F (1998) Novel applications and implementations of shape deposition manufacturing. *Naval Research Reviews, Office of Naval Research* 1
- Cham J, Pruitt B, Cutkosky M, Binnard M, Weiss L, Neplotnik G (1999) Layered manufacturing with embedded components: process planning considerations. *Proceedings of DETC99: 1999 ASME Design Engineering Technical Conference*
- Palmer JA, Yang P, Davis DW, Chavez BD, Gallegos PL, Wicker RB, Medina F (2004) Rapid prototyping of high density circuitry. *Proceedings of the Rapid Prototyping & Manufacturing 2004 Conference*
- Medina F, Lopes AJ, Inamdar AV, Hennessey R, Palmer JA, Chavez BD, Wicker RB (2005a) Integrating multiple rapid manufacturing technologies for developing advanced customized functional devices. *Rapid Prototyping & Manufacturing 2005 Conference Proceedings* 10–12
- Medina F, Lopes AJ, Inamdar AV, Hennessey R, Palmer JA, Chavez BD, Davis D, Gallegos P, Wicker RB (2005b) Hybrid manufacturing: integrating stereolithography and direct write technologies. *16th Annual International Solid Freeform Fabrication Symposium*. pp. 39–49
- Lopes AJ, Navarrete M, Medina F, Palmer J, MacDonald E, Wicker RB (2006) Expanding rapid prototyping for electronic systems integration of arbitrary form. *17th Annual International Solid Freeform Fabrication Symposium*
- Palmer JA, Davis DW, Gallegos PL, Yang P, Chavez BD, Medina F, Wicker RB (2005) Stereolithography: a basis for integrated meso manufacturing. *16th Annual Solid Freeform Fabrication Symposium*. pp. 476–483
- Malone E, Lipson H (2006) Freeform fabrication of ionomeric polymer-metal composite actuators. *Rapid Prototyp J* 12:244–253. doi:[10.1108/13552540610707004](https://doi.org/10.1108/13552540610707004)
- Malone E, Berry M, Lipson H (2008) Freeform fabrication and characterization of Zn-air batteries. *Rapid Prototyp J* 14:128–140. doi:[10.1108/13552540810877987](https://doi.org/10.1108/13552540810877987)
- Periard D, Malone E, Lipson H (2007) Printing embedded circuits. *18th Annual International Solid Freeform Fabrication Symposium*. pp. 503–512
- Navarrete M, Lopes A, Acuna J, Estrada R, MacDonald E, Palmer J, Wicker R (2007) Integrated layered manufacturing of a novel wireless motion sensor system with GPS. *18th Annual International Solid Freeform Fabrication Symposium*. pp. 575–585
- Ram GDJ, Robinson C, Yang Y, Stucker BE (2007) Use of ultrasonic consolidation for fabrication of multi-material structures. *Rapid Prototyp J* 13:226–235. doi:[10.1108/13552540710776179](https://doi.org/10.1108/13552540710776179)
- DeGrange J, Macy B (2012) Smart parts: Additive manufacturing for integrated electro-mechanical devices [webinar]. Retrieved from <http://www.stratasys.com/Resources/Webinars/Smart-Parts.aspx>
- Paulsen JA, Renn M, Christenson K, Plourde R (2012) Printing conformal electronics on 3D structures with Aerosol Jet technology. *Future of Instrumentation International Workshop (FIIW)*, 2012. pp 1–4
- Chrisey DB, Piqué A (2002) Direct-write technologies for rapid prototyping applications: sensors, electronics, and integrated power sources. Academic, CA
- Piqué A, Mathews SA, Pratap B et al (2006) Embedding electronic circuits by laser direct-write. *Microelectron Eng* 83:2527–2533. doi:[10.1016/j.mee.2006.06.004](https://doi.org/10.1016/j.mee.2006.06.004)
- DARPA DSO (2010) <http://www.darpa.mil/dso/archives/mice/> (accessed 28 May 2010)
- Kim D, Moon J (2005) Highly conductive ink jet printed films of nanosilver particles for printable electronics. *Electrochim Solid-State Lett* 8:J30–J33. doi:[10.1149/1.2073670](https://doi.org/10.1149/1.2073670)
- Jagt JC (1998) Reliability of electrically conductive adhesive joints for surface mount applications: a summary of the state of the art.

- IEEE Transact Components Packaging, and Manufacturing Technology, Part A 21:215–225. doi:[10.1109/95.705467](https://doi.org/10.1109/95.705467)
32. Greer JR, Street RA (2007) Thermal cure effects on electrical performance of nanoparticle silver inks. *Acta Mater* 55:6345–6349. doi:[10.1016/j.actamat.2007.07.040](https://doi.org/10.1016/j.actamat.2007.07.040)
33. Park BK, Kim D, Jeong S et al (2007) Direct writing of copper conductive patterns by ink-jet printing. *Thin Solid Films* 515:7706–7711. doi:[10.1016/j.tsf.2006.11.142](https://doi.org/10.1016/j.tsf.2006.11.142)
34. De Nava E, Muse D, Castillo S, Alawneh M, Navarrete M, Lopes AJ, MacDonald E, Wicker RB (2008) Three-dimensional off-axis component placement and routing with solid freeform fabrication. Proceedings from the 19th Annual Solid Freeform Fabrication Symposium. Austin, TX, pp 362–369
35. Olivas R, Salas R, Muse D, MacDonald E, Wicker R (2010) Structural electronics through additive manufacturing and micro-dispensing” International Microelectronics Assembly and Packaging Society Nationals Conference
36. Mireles J (2013) Development of a fused deposition modeling system for low melting temperature metal alloys. *J Electron Packag* 135: 011008. doi:[10.1115/1.4007160](https://doi.org/10.1115/1.4007160)
37. Auyeung CY, Kim H, Mathew SA, Pique A (2007) Laser direct-write of metallic nanoparticle inks. *J Laser Micro-Nanoeng (JLMN)* 2007: 21–25
38. Schroder KA, McCool SC, Furlan WF (2006) Broadcast photonic curing of metallic nanoparticle films. Technical Proceedings of the 2006 NSTI Nanotechnology Conference and Trade Show. pp. 198–201
39. Kief C J, Zufelt BK, Christensen JH, Mee JK (2011) Trailblazer: proof of concept CubeSat Mission for SPA-1. American Institute of Aeronautics and Astronautics Infotech. pp. 1–7
40. National Aeronautics and Space Administration (NASA) (2013) Outgassing data for selecting spacecraft materials. Retrieved from <http://outgassing.nasa.gov/>
41. CubeSat Design Specification Rev. 12 (2010) California State Polytechnic University. Retrieved 2010-10-16
42. Steinhögl W, Schindler G, Steinlesberger G, Engelhardt M (2002) Size-dependent resistivity of metallic wires in the mesoscopic range. *Phys Rev B* 66:075414. doi:[10.1103/PhysRevB.66.075414](https://doi.org/10.1103/PhysRevB.66.075414)
43. Salam B, Lai WL, Albert LCW, Keng LB (2011) Low temperature processing of copper conductive ink for printed electronics applications. Electronics Packaging Technology Conference (EPTC), 2011 I.E. 13th. pp 251–255
44. Lee B, Kim Y, Yang S, Jeong I, Moon J (2009) A low-cure-temperature copper nano ink for highly conductive printed electrodes. *Curr Appl Phys* 9:e157–e160. doi:[10.1016/j.cap.2009.03.008](https://doi.org/10.1016/j.cap.2009.03.008)
45. Wohlers TT (2012) Wohlers report 2012, rapid prototyping, tooling and manufacturing: state of the industry. Annual Worldwide Progress Report, Wohlers Associates Inc., Colorado
46. Wu KC, Halloran JW (2005) Photopolymerization monitoring of ceramic stereolithography resins by FTIR methods. *J Mater Sci* 40: 71–76. doi:[10.1007/s10853-005-5689-y](https://doi.org/10.1007/s10853-005-5689-y)
47. Zeon, 2011. ZEONEX RS420 datasheet. <http://www.zeonchemicals.com/newcustomer.aspx?returnURL=/docServer.aspx?f=MjI5NjQyNTc=>
48. Knowles MRH, Rutherford G, Karnakis D, Ferguson A (2007) Micro-machining of metals, ceramics and polymers using nanosecond lasers. *Int J Adv Manuf Technol* 33:95–102. doi:[10.1007/s00170-007-0967-2](https://doi.org/10.1007/s00170-007-0967-2)
49. Espalin D, Ramirez J, Medina F, Wicker R (2012) Multi-material, multi-technology FDM system. 23rd Annual International Solid Freeform Fabrication Symposium. pp. 828–835, August 2012, Austin
50. Espalin D, Ramirez J, Medina F, Wicker R (2014) Multi-material, multi-technology FDM: exploring build process variations. *Rapid Prototyp J* 20
51. Dupont, 2009. Dupont CB028 datasheet. http://www2.dupont.com/MCM/en_US/assets/downloads/prodinfo/CB028.pdf
52. Dupont, 2010. Dupont CB500 datasheet. http://www2.dupont.com/MCM/en_US/assets/downloads/prodinfo/CB500_ProcessingGuide.pdf
53. Roberson DA, Wicker RB, MacDonald E (2012) Ohmic curing of printed silver conductive traces. *J Electron Mater* 41:2553–2566. doi:[10.1007/s11664-012-2140-4](https://doi.org/10.1007/s11664-012-2140-4)
54. Kapton polyimide film datasheet. http://www2.dupont.com/Kapton/en_US/
55. Shengyi S1141. www.agssales.com/pcb-datasheets-shengyi.html
56. Machinability Data Center (1980) Milling operations. Machining data handbook, Metcut Research Associates Inc., Ohio. pp. 2–1 – 2–233
57. Kibbe RR, Neely JE, Meyer RO, White WT (1982) Vertical milling machines, machine tool practices. Wiley, New York
58. Top 10 design tips for injection-molded parts: complete with material options and tolerances (2013) Guttenberg Industries Inc
59. Boschetto A, Giordano V, Veniali F Surface roughness prediction in fused deposition modelling by neural networks. *Int J Adv Manuf Technol* 1–16. doi:[10.1007/s00170-012-4687-x](https://doi.org/10.1007/s00170-012-4687-x)
60. Jan J-Y, Tseng L-C (2004) Small planar monopole antenna with a shorted parasitic inverted-L wire for wireless communications in the 2.4-, 5.2-, and 5.8-GHz bands. *IEEE Trans Antennas Propag* 52: 1903–1905. doi:[10.1109/TAP.2004.831370](https://doi.org/10.1109/TAP.2004.831370)